nature materials

LETTERS

PUBLISHED ONLINE: 17 NOVEMBER 2014 | DOI: 10.1038/NMAT4140

Synthesis of an open-framework allotrope of silicon

Duck Young Kim[1†], Stevce Stefanoski[1†], Oleksandr O. Kurakevych[1,2†] and Timothy A. Strobel[1*†]

Silicon is ubiquitous in contemporary technology. The most stable form of silicon at ambient conditions takes on the structure of diamond (cF8, *d*-Si) and is an indirect bandgap semiconductor, which prevents it from being considered as a next-generation platform for semiconductor technologies[1–4]. Here, we report the formation of a new orthorhombic allotrope of silicon, Si_{24}, using a novel two-step synthesis methodology. First, a Na_4Si_{24} precursor was synthesized at high pressure[5]; second, sodium was removed from the precursor by a thermal 'degassing' process. The *Cmcm* structure of Si_{24}, which has 24 Si atoms per unit cell (*o*C24), contains open channels along the crystallographic *a*-axis that are formed from six- and eight-membered sp^3 silicon rings. This new allotrope possesses a quasidirect bandgap near 1.3 eV. Our combined experimental/theoretical study expands the known allotropy for element fourteen and the unique high-pressure precursor synthesis methodology demonstrates the potential for new materials with desirable properties.

Silicon is the second most abundant element in the Earth's crust, existing naturally within various oxygen-rich minerals. Purified silicon is an essential ingredient of modern technology as it is used widely for a great deal of electronic devices. This common material takes on the cubic diamond structure, which is the thermodynamic ground state at ambient conditions. The tetrahedral bonding in silicon provides a very complex energy landscape with numerous hypothetical allotropes possessing very small energy differences from the ground state[4,6–8]. Multiple allotropes have been discovered under high-pressure conditions[9], including two metastable phases that are recoverable to ambient pressure[10]. In addition, chemical methods have been shown to produce new silicon structures, such as the guest-free modification of type-II silicon clathrate[11–13] and *allo*-Si (ref. 14).

Silicon is a mainstay of semiconductor technology because of the elemental abundance, relatively low costs, ability for doping by other elements, and a native oxide passivation layer. The direct bandgap of *d*-Si (3.2 eV) is much wider than the indirect gap (1.17 eV), and thus phonons are needed to mediate electronic excitations from visible and infrared light. This limitation prevents silicon from being considered as a next-generation, high-efficiency platform for applications such as light-emitting diodes[1,3], higher-performance transistors[2], as well as thin-film photovoltaic devices[4].

Studies have been motivated by the potential to find new silicon allotropes with advanced optical and electronic properties beyond those of *d*-Si (refs 4,7,15–17). In particular, photovoltaic applications ideally require a direct bandgap of ~1.3 eV (ref. 18), which has not been achieved by any existing silicon phase. Theoretically, low-energy silicon allotrope candidates were suggested that exhibit greatly improved visible light absorption characteristics with quasidirect bandgaps (nearly degenerate indirect and direct gaps)[4,7]; however, no experimental synthesis has been reported thus far. Of the known metastable Si allotropes, the BC8 structure is probably semi-metallic[16], and the R8 structure was calculated to possess a small indirect gap of 0.24 eV (ref. 15). Lonsdaleite silicon, produced by heating the BC8 structure above 470 K, has an indirect gap of ~1 eV (refs 15,16) and the crystal structure of *allo*-Si is not clearly resolved[19]. Type-II silicon clathrate, Si_{136}, possesses a wide bandgap of 1.9 eV (ref. 17), and symmetry analysis of the cubic Si_{136} structure shows that electric dipole transitions associated with this gap are forbidden[20].

Silicon-rich compounds may be considered as another route for synthesizing novel classes of silicon allotropes. This approach was used previously for the synthesis of type-II silicon clathrate[12] and germanium clathrate[19], both of which use chemical precursors that are formed at ambient pressure. But what if compounds recovered from high-pressure conditions were used as chemical precursors instead of compounds formed at ambient pressure? In this case, the synthesis of entirely new, previously inaccessible phases may become possible by performing ambient-pressure chemical manipulations on inherently metastable materials recovered from high pressure, owing to the increased metastability on recovery and access to entirely different regions of phase space.

Recently, we reported the formation of Na_4Si_{24} (unit cell composition, which can be described as four formula units of $NaSi_6$) above ~8 GPa (ref. 5) and the concomitant metastable recovery of this phase to ambient conditions. Na_4Si_{24} possesses the $Eu_4Ga_8Ge_{16}$ (ref. 21) type structure also found in $BaSi_6$ (ref. 22), $SrSi_6$ (ref. 23), $CaSi_6$ (ref. 24) and $EuSi_6$ (ref. 25). This compound consists of a channel-like sp^3 silicon host structure filled with linear Na chains as a guest structure. These open channels that host Na suggest a possible pathway for Na removal via diffusion along the channels, as schematically shown in Fig. 1a.

By exposing recovered Na_4Si_{24} samples to elevated temperatures, removal of Na from the structure was observed. This process occurs at temperatures as low as 320 K, whereas type-II silicon clathrates (Na_xSi_{136}) require much higher temperatures (>623 K) for Na removal[12,26]. Thermal 'degassing' of Na_4Si_{24} at 400 K under dynamic vacuum resulted in a gradual reduction of the Na content—with Na being completely removed from the structure over a period of eight days. Figure 2a shows powder X-ray diffraction (PXRD) patterns obtained from Na_4Si_{24} and from a sample recovered after the thermal 'degassing' process. After the eight-day period the host structure remains unchanged (*Cmcm*); however, the lattice parameters and PXRD peak intensities are significantly different. The best Rietveld fits were obtained when sodium was excluded from the refinement

[1]Geophysical Laboratory, Carnegie Institution of Washington, Washington DC 20015, USA. [2]IMPMC, UPMC Sorbonne Universités, UMR CNRS 7590, Muséum National d'Histoire Naturelle, IRD UMR 206, 75005 Paris, France. †These authors contributed equally to this work. *e-mail: tstrobel@ciw.edu

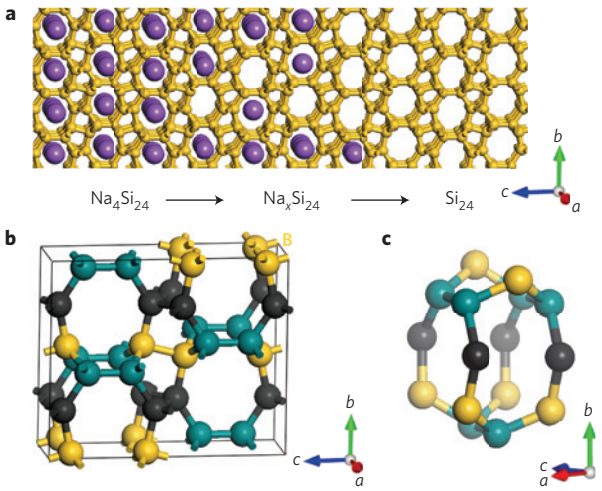

Figure 1 | Crystal structures of Na_4Si_{24} and Si_{24}. a, Schematic of the compositional change from Na_4Si_{24} (left) to Si_{24} (right). Sodium atoms are shown in purple and silicon atoms in yellow. **b**, Si_{24} unit cell exhibiting three crystallographically unique positions in each colour. **c**, Fractional view of Si_{24} emphasizing its channel structure. Channels are formed by eight-member rings along the *a*-axis, which are linked by six-membered rings on the top and sides. These channels are connected along the *c*-axis by five-membered rings.

(including Na led to negative site occupancies with non-physical displacement parameters), indicating that the sodium concentration is below the detectable limits using PXRD. Excellent agreement between the experimental and calculated lattice parameters, for both full and empty structures, provides further support for the removal of the Na in the Si_{24} structure (Fig. 2c). By removing Na, the *a*, *b* and *c* lattice parameters change by −6.8%, +1.2% and +3.0%, respectively, which indicates that the void channel diameters become larger and the length along the channels is reduced on Na removal. Furthermore, the Raman spectrum for the Na-free Si_{24} structure is much different from Na_4Si_{24} (and in excellent agreement with theoretical predictions), corroborating the absence of Na from the Si_{24} structure (Supplementary Information).

The absence of sodium was also demonstrated using energy-dispersive X-ray spectroscopy (EDXS). EDXS measurements were performed on 'degassed' samples of Na_xSi_{24} ($0 \leq x \leq 4$) (Fig. 2b). No sodium was detected in the EDXS spectrum for completely degassed samples, indicating that the sodium content is below the detection limit of the instrument (<0.1 atom%). Thus, the new phase is at least 99.9% pure silicon and may be considered as a new allotrope: Si_{24}(*o*C24).

Si_{24} possesses an orthorhombic structure (space group *Cmcm*, no. 63) with lattice parameters $a = 3.82236(14)$ Å, $b = 10.7007(4)$ Å and $c = 12.6258(5)$ Å. There are three non-equivalent Si positions (Supplementary Information) and each Si atom is connected tetrahedrally with bond lengths ranging from 2.33 to 2.41 Å, as compared to the bond length of *d*-Si (2.35 Å). Along the *a*-axis, Si_{24} possesses octagonal linear channels, which were occupied by Na in Na_4Si_{24}. To maintain the void space, the bond angles are distorted in a range from 93.7° to 135.9°, deviating from the perfect tetrahedral angle (109.5°). The low density of Si_{24} (2.17 g cm^{-3}), due to its open framework, is between that of *d*-Si (2.33 g cm^{-3}) and Si_{136} clathrate (2.15 g cm^{-3}). Interestingly, Si_{24} exhibits the same topology as the zeolite type with International Zeolite Association (IZA) code CAS (ref. 27), and the corresponding CAS-Si crystal structure was previously suggested on the basis of density functional theory (DFT) calculations[28]. In fact, it is common to use various inorganic/organic templates for controlling pores in zeolite synthesis[29], and we speculate that our high-pressure precursor approach may be applied to find Si allotropes with other zeolite structures.

The thermodynamic and dynamic stability of the new silicon phase was investigated using first-principles calculations. Total energy calculations using DFT show that Si_{24} possesses an enthalpy higher than *d*-Si by 0.09 eV/atom and is energetically more favourable than other known metastable BC8 and R8 phases[4]. Phonon dispersion relations for Si_{24}, obtained from lattice dynamics calculations (Supplementary Information), indicate that this structure is dynamically stable at both high- and low-pressure conditions. This fact demonstrates that the removal of sodium atoms from Na_4Si_{24} does not affect the lattice stability of the Si framework. At ambient pressure, the Si_{24} lattice maintains dynamic stability, which is consistent with our experimental observations at ambient conditions. In our calculations, Si_{24} is destabilized above 10 GPa and we speculate that it might transform to the metallic Si-II (β-tin) structure, similar to type-II Si clathrate, above 12 GPa (ref. 30). PXRD measurements indicate that Si_{24} decomposes near 750 K when heated in air (Supplementary Information).

To gain further insights into the properties of Si_{24}, the electronic band structure was calculated. Using DFT (Perdew–Burke–Ernzerhof (PBE)), Si_{24} was calculated to have a direct bandgap (E_d) of 0.57 eV and an indirect bandgap (E_i) of 0.53 eV (Supplementary Information). The difference between E_d and E_i is small, albeit formally an indirect bandgap material. The highest valence and the lowest conduction bands are very flat in the Γ–Z direction, indicating a quasidirect gap nature for Si_{24}. It is a well-known limitation of standard DFT to underestimate the bandgap of silicon. Therefore, we used quasiparticle (G_0W_0) calculations for accurate bandgap estimations. Under this approach, we successfully reproduced the indirect gap value of 1.12 eV for *d*-Si (1.17 eV from experiment) and found that the G_0W_0-corrected E_d and E_i for Si_{24} are 1.34 eV and 1.30 eV, respectively (Fig. 3a,b). It is worth noting that the indirect gap nature of Si_{24} can be easily tuned to a formally direct gap material by uniaxial compression (strain engineering). As the conduction band minimum is located at the Z point and the valence band maximum is at the Γ point, our calculations show that a two per cent lattice compression along the *c*-axis induces an indirect-to-direct gap transition (Supplementary Information).

The temperature dependence of the electrical conductivity, σ, for Si_{24} is shown in Fig. 3c. Si_{24} exhibits semiconducting behaviour, where σ increases with increasing T. This is in contrast to the temperature dependence of σ for Na_4Si_{24} (ref. 5), which is metallic owing to the excess charge carriers associated with Na. The rigid-band model, applicable to other guest–host compounds[31], can be also applied to Na_xSi_{24} ($0 \leq x \leq 4$). According to this model, the electropositive Na donates its valence electrons to the conduction bands of the Si framework. Si_{24}, as compared to Na_4Si_{24}, has no available conduction charge carriers and, therefore, exhibits semiconducting behaviour (Fig. 3c). Using DFT, we calculated the electronic structure of Na_xSi_{24} down to $x = 0.125$ (~0.5 atom%) and found that this small Na content is enough to maintain the metallic nature of the compound (Supplementary Information). Thus, a metal-to-semiconductor transition is observed when sodium is completely removed from the structure. A bandgap of 1.3 eV was calculated for Si_{24} from the intrinsic region of the electrical conductivity (Fig. 3c), which is in excellent agreement with our G_0W_0 calculations.

Optical reflectivity measurements were performed on samples of Si_{24} to obtain absorption information from the powder samples and to further evaluate the bandgap. Figure 3d shows Tauc plots[32] of the Kubelka–Munk absorption (K/S) with the data scaled for both indirect and direct transitions. If a plot of $(K/S \cdot h\nu)^{1/2}$ versus $h\nu$ yields a straight line, E_i can be estimated by extrapolating this line to $K/S = 0$. Similarly, E_g is estimated from a plot of $(K/S \cdot h\nu)^2$ versus $h\nu$. Under this approach, absorption edges for Si_{24} were observed

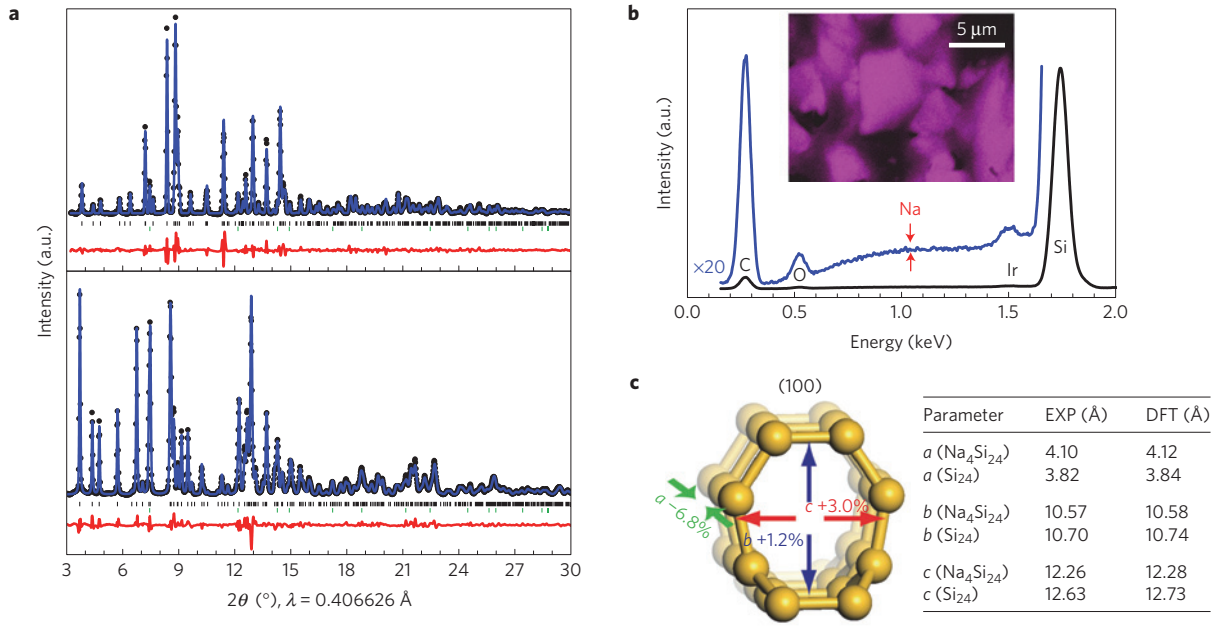

Parameter	EXP (Å)	DFT (Å)
a (Na_4Si_{24})	4.10	4.12
a (Si_{24})	3.82	3.84
b (Na_4Si_{24})	10.57	10.58
b (Si_{24})	10.70	10.74
c (Na_4Si_{24})	12.26	12.28
c (Si_{24})	12.63	12.73

Figure 2 | Structure determination and composition information for Si_{24}. a, PXRD data (points) and Rietveld refinements (blue lines) for Na_4Si_{24} (top) and Si_{24} (bottom). Red lines indicate the difference between experimental data and refinement. Black tick marks indicate reflection positions for Na_4Si_{24} (top) and Si_{24} (bottom). Green tick marks indicate reflection positions for *d*-Si (~3 wt% impurity). **b**, EDXS spectrum obtained from an iridium-coated Si_{24} sample. No sodium is detected (position of red arrows). Carbon and oxygen originate from organic contamination and a native oxide layer, respectively. Inset shows an SEM/EDXS mapping image of ~5 µm crystals. Purple colour indicates silicon. **c**, Effect of sodium removal on the lattice parameters and a table of measured (EXP) and calculated (DFT) lattice parameters for Na_4Si_{24} and Si_{24}.

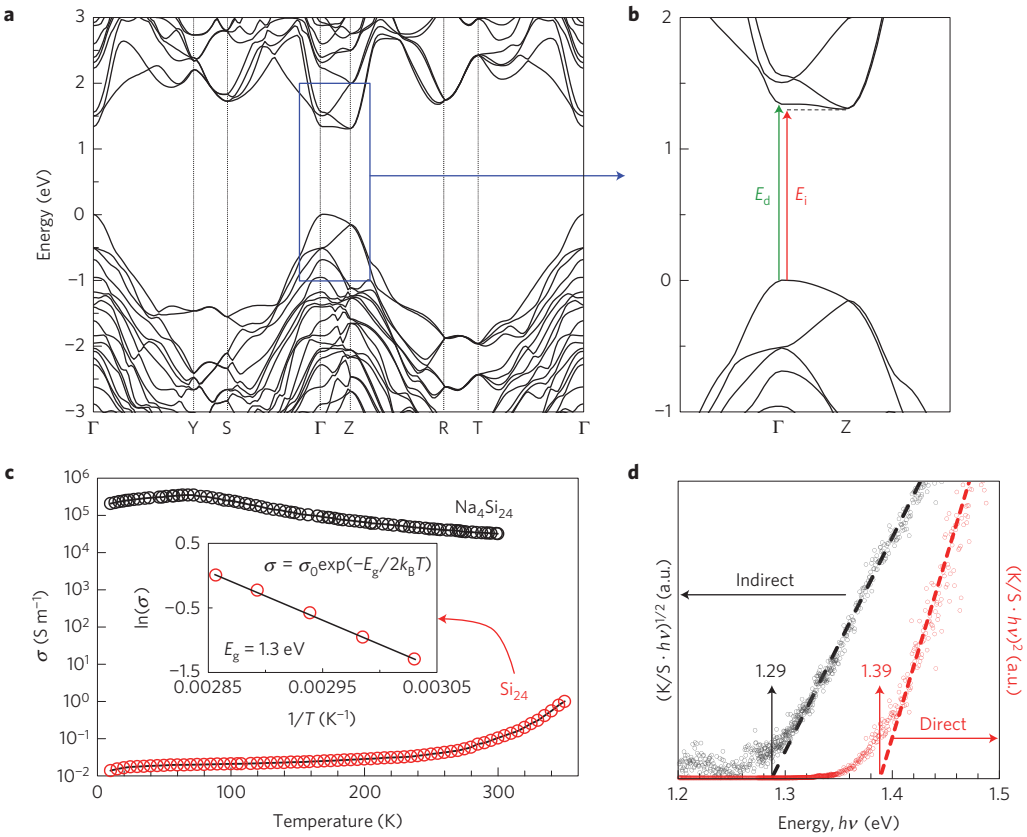

Figure 3 | Electronic and optical properties of Si_{24}. a, Calculated Si_{24} band structure (PBE+G_0W_0). **b**, Zoomed-in region of the bandgap. Arrows indicate direct (E_d) and indirect (E_i) gaps. **c**, Electrical conductivity σ as a function of temperature T of Na_4Si_{24} and Si_{24} (inset shows the fit of the intrinsic conductivity region with a bandgap of 1.3 eV). **d**, Tauc plots of Kubelka–Munk absorption (K/S) as a function of energy, $h\nu$ for Si_{24} obtained from optical reflectivity measurements. Absorption edges are observed at 1.29 eV and 1.39 eV assuming indirect and direct electronic transitions, respectively.

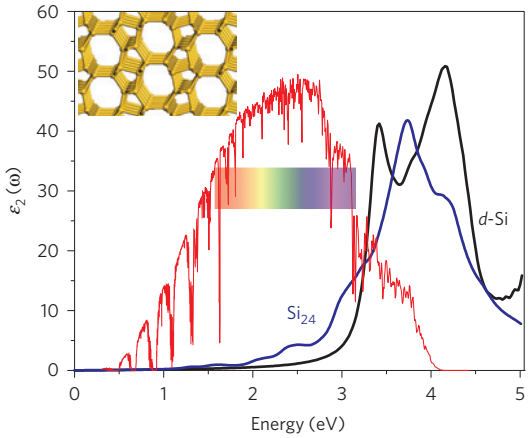

Figure 4 | Absorption spectra. Calculated BSE absorption (ε_2) for Si_{24} (blue) and *d*-Si (black) compared with the reference air mass (AM) 1.5 solar spectral irradiance (red).

at 1.29 eV and 1.39 eV, assuming indirect and direct transitions, respectively. Although single-crystal or thin-film samples should be measured for a more strict discussion of the bandgap, the observed absorption edges are in excellent agreement with the energy gaps determined from electrical conductivity measurements and from theoretical estimates using first-principles calculations (Supplementary Information). These various methods constrain the bandgap of Si_{24} near 1.3 eV and indicate only a minor separation between the direct and indirect values: 0.04 eV from the G_0W_0 calculation, ~0.1 eV from experiment.

To check for potential improvements in light absorption properties, we calculated absorption spectra (imaginary part of dielectric function, ε_2) of Si_{24}, as shown in Fig. 4, compared with *d*-Si, by solving the Bethe–Salpeter equation (BSE; refs 33,34). The absorption of these two phases is compared with the reference air mass (AM) 1.5 solar spectral irradiance[35]. Compared with *d*-Si, the light absorption of Si_{24} is significantly enhanced below 3 eV, particularly in the visible light range where solar spectral irradiation has its maximum intensity. Whereas the electric dipole transitions at the bandgap of Si_{136} are forbidden by symmetry[20], optical absorption in Si_{24} starting from the absorption edge is dipole allowed. It is interesting to note that the calculated absorption intensity of Si_{24} is quantitatively comparable to that of ternary chalcopyrite semiconductor compounds ($CuInSe_2$, $CuGaSe_2$; ref. 36), which are well-known thin-film solar cell materials[4].

In conclusion, we have presented the discovery of a new allotrope of silicon, Si_{24}, formed through a novel high-pressure precursor process. The sodium concentration was found to be <0.1 atom%—our laboratory detection limit. Electrical resistivity and optical reflectivity measurements indicate that Si_{24} is a semiconductor with a bandgap of ~1.3 eV, in excellent agreement with our first-principles calculations. The difference between E_d and E_i is negligibly small (<0.1 eV) and both are well within the optical bandgaps for photovoltaic applications (<1.5 eV), which is a unique property of this new silicon allotrope. It is interesting that the bandgap of Si_{24} coincides with the theoretically proposed optimal value that maximizes solar conversion efficiency for a single p–n junction to 33.7%, namely the 'Shockley–Queisser limit'[18]. Therefore, Si_{24} seems to be a promising candidate for thin-film solar applications, which should be investigated further along with other properties such as carrier mobility and the potential for light emission. The quasidirect nature of the bandgap allows greatly improved optical properties, while the material maintains the advantages of silicon—for example, the potential for doping, an oxide layer, and so on. The synthesis of Si_{24} at present requires a high-pressure precursor, which places limitations on scalability for eventual applications. However, low-pressure methods such as chemical vapour deposition could potentially enable larger scale production of Si_{24}, as is the case for diamond[37], another high-pressure phase. Furthermore, the unique zeolite-like nature of this structure provides another perspective for synthesizing new low-density polymorphs in other classes of materials[38], which would be of interest for gas and/or lithium storage and for molecular-scale filtering applications[39]. More broadly, Si_{24} expands the known allotropy in element fourteen and the novel high-pressure precursor synthesis approach suggests the potential for entirely new materials with desirable properties.

Methods

Synthesis. Si_{24} was synthesized in a two-step process. In the first step, Na_4Si_{24} was synthesized from a Na/Si mixture with 15 mol% Na. The mixture was ground in a ceramic mortar for one hour inside a high-purity Ar glovebox and loaded into a Ta capsule (or h-BN capsule for probing with synchrotron radiation). The capsule was then introduced in a 14/8 multianvil assembly using a Re heater and ZrO_2 insulation (graphite and MgO, respectively, for synchrotron-assisted syntheses). Shorting between Ta and Re was prevented by employing Al_2O_3 tubes, and a W–Re C-type thermocouple, imbedded in an Al_2O_3 plug, was used for accurate temperature control. The mixture was pressurized in a 1500 ton multianvil press at a rate of 10 bar h^{-1} (oil pressure) to a pressure of 10 GPa and reacted at 800 °C in two steps: preheating at 400 °C for 30 min, to avoid a blow-out of the overheated Na, and reaction at the final temperature for one hour, after which the sample was quenched by switching off the power. The recovered sample was easily removed from the Ta capsule and then washed with distilled water. The resulting product of the reaction was polycrystalline Na_4Si_{24}. In the second step, polycrystalline agglomerates of Na_4Si_{24} were placed in a furnace under a dynamic vacuum of ~10^{-5} torr and 'degassed' at 400 K for eight days to obtain the empty Si_{24} structure, which was subsequently washed thoroughly with water.

Powder X-ray diffraction. Angular dispersive PXRD data were collected at HPCAT (sector 16) of the Advanced Photon Source, Argonne National Laboratory using a monochromatic beam (~$10 \times 10\,\mu m^2$) with an energy of 30.5 keV. Two-dimensional diffraction data were collected using a Pilatus detector and integrated using the FIT2D software, calibrated using a high-purity CeO_2 standard. Rietveld refinements were carried out using GSAS with the EXPGUI software.

Monochromatic X-ray diffraction data were also taken at beamline ID06 of the ESRF using a wavelength corresponding to 33/55 keV, which was selected from the emission of a u18 cryogenic undulator with a Si(111) double-crystal monochromator. The beam was collimated to define a horizontal beam size of ~1 mm to assure probing of the whole sample. Pressures were generated and regulated using the 20MN Voggenreiter cubic press LPO 2000-1000/20, where the vertical-acting piston loads were monitored to ensure triaxial loading at all pressure points.

Laboratory PXRD data for thermal stability studies in air were acquired using a Bruker D8 Discover equipped with a microfocus source (Cu Kα) and Vantec500 area detector.

Electron microscopy. EDXS measurements were performed using a JEOL JSM-6500F microscope equipped with an Oxford Instruments X-max detector (80 mm^2) and the data were analysed using the Aztec software.

Electrical measurements. Electrical resistivity was measured with a Physical Property Measurement System (PPMS) from Quantum Design using a two-probe method. Platinum wires (5 μm) were attached to the dense polycrystalline specimens (~50 μm in size) using Leitsilber conductive silver cement (Ted Pella, silver content 45%, sheet resistance: 0.02–0.04 $\Omega\,\square^{-1}$).

Optical reflectivity. Optical reflectivity measurements were performed on polycrystalline powder samples of Si_{24} using the near/mid infrared light source from an Agilent Cary 670 spectrometer. Reflected light was focused into a dispersive spectrometer with a charge-coupled device detector. A PTFE standard was used as a reflectance reference. Reflectivity data were processed under the Kubelka–Munk formalism and bandgaps were estimated from Tauc plots.

First-principles calculations. For accurate bandgap estimations, we have employed quasiparticle calculations (GW) and a hybrid functional approach (HSE06) for a comparison. We used Bethe–Salpeter equation (BSE) to compute the Coulomb correlation between the photoexcited electrons and holes. Full details of the first-principles calculations, with complete references, can be found in the Supplementary Information.

Received 8 May 2014; accepted 13 October 2014; published online 17 November 2014

References

1. Ng, W. L. *et al.* An efficient room-temperature silicon-based light-emitting diode. *Nature* **410,** 192–194 (2001).
2. Theis, T. N. & Solomon, P. M. It's time to reinvent the transistor. *Science* **327,** 1600–1601 (2010).
3. Fujita, M. Silicon photonics: Nanocavity brightens silicon. *Nature Photon.* **7,** 264–265 (2013).
4. Botti, S., Flores-Livas, J. A., Amsler, M., Goedecker, S. & Marques, M. A. L. Low-energy silicon allotropes with strong absorption in the visible for photovoltaic applications. *Phys. Rev. B* **86,** 121204(R) (2012).
5. Kurakevych, O. O., Strobel, T. A., Kim, D. Y., Muramatsu, T. & Struzhkin, V. V. Na–Si clathrates are high-pressure phases: A melt-based route to control stoichiometry and properties. *Cryst. Growth Des.* **13,** 303–307 (2012).
6. Zwijnenburg, M. A., Jelfs, K. E. & Bromley, S. T. An extensive theoretical survey of low-density allotropy in silicon. *Phys. Chem. Chem. Phys.* **12,** 8505–8512 (2010).
7. Xiang, H. J., Huang, B., Kan, E., Wei, S-H. & Gong, X. G. Towards direct-gap silicon phases by the inverse band structure approach. *Phys. Rev. Lett.* **110,** 118702 (2013).
8. Malone, B. D. & Cohen, M. L. Prediction of a metastable phase of silicon in the *Ibam* structure. *Phys. Rev. B* **85,** 024116 (2012).
9. Tonkov, E. Y. & Ponyatovsky, E. G. *Phase Transformations of Elements Under High Pressure* (CRC Press, 2005).
10. Wentorf, R. H. & Kasper, J. S. Two new forms of silicon. *Science* **139,** 338–339 (1963).
11. Cros, C., Pouchard, M. & Hagenmuller, P. Sur deux nouvelles phases du système silicium-sodium. *C. R. Acad. Sci.* **260,** 4764–4767 (1965).
12. Gryko, J. *et al.* Low-density framework form of crystalline silicon with a wide optical band gap. *Phys. Rev. B* **62,** R7707–R7710 (2000).
13. Kasper, J. S., Hagenmuller, P., Pouchard, M. & Cros, C. Clathrate structure of silicon Na_8Si_{46} and Na_xSi_{136} ($x < 11$). *Science* **150,** 1713–1714 (1965).
14. Schnering, H. V., Schwarz, M. & Nesper, R. The lithium sodium silicide Li_3NaSi_6 and the formation of allo-silicon. *J. Less-Common Met.* **137,** 297–310 (1988).
15. Malone, B. D., Sau, J. D. & Cohen, M. L. *Ab initio* survey of the electronic structure of tetrahedrally bonded phases of silicon. *Phys. Rev. B* **78,** 035210 (2008).
16. Besson, J. M., Mokhtari, E. H., Gonzalez, J. & Weill, G. Electrical properties semimetallic silicon III and semiconductive silicon IV at ambient pressure. *Phys. Rev. Lett.* **59,** 473–476 (1987).
17. Dong, J., Sankey, O. F. & Kern, G. Theoretical study of the vibrational modes and their pressure dependence in the pure clathrate-II silicon framework. *Phys. Rev. B* **60,** 950–958 (1999).
18. Shockley, W. & Queisser, H. J. Detailed balance limit of efficiency of pn junction solar cells. *J. Appl. Phys.* **32,** 510–519 (1961).
19. Guloy, A. M. *et al.* A guest-free germanium clathrate. *Nature* **443,** 320–323 (2006).
20. Connétable, D. Structural and electronic properties of p-doped silicon clathrates. *Phy. Rev. B* **75,** 125202 (2007).
21. Bryan, J. D. & Stucky, G. D. $Eu_4Ga_8Ge_{16}$: A new four-coordinate clathrate network. *Chem. Mater.* **13,** 253–257 (2001).
22. Yamanaka, S. & Maekawa, S. Structural evolution of the binary system Ba–Si under high-pressure and high-temperature conditions. *Z. Naturforsch.* **61,** 1493–1499 (2006).
23. Wosylus, A. *et al.* High-pressure synthesis of strontium hexasilicide. *Z. Naturforsch.* **61,** 1485–1492 (2006).
24. Wosylus, A., Prots, Y., Burkhardt, U., Schnelle, W. & Schwarz, U. High-pressure synthesis of the electron-excess compound $CaSi_6$. *Sci. Technol. Adv. Mater.* **8,** 383–388 (2007).
25. Wosylus, A. *et al.* Breaking the Zintl rule: High-pressure synthesis of binary $EuSi_6$ and its ternary derivative $EuSi_{6-x}Ga_x$ ($0 \leq x \leq 0.6$). *Solid State Sci.* **8,** 773–781 (2006).
26. Stefanoski, S., Malliakas, C. D., Kanatzidis, M. G. & Nolas, G. S. Synthesis and structural characterization of Na_xSi_{136} ($0 < x \leq 24$) single crystal and low-temperature transport of polycrystalline specimens. *Inorg. Chem.* **51,** 8686–8692 (2012).
27. Baerlocher, Ch., McCusker, L. B. & Olson, D. H. *Atlas of Zeolite Framework Types* 6th revised edn, Vol. 86 (Elsevier, 2007).
28. Conesa, J. C. Computer modeling of allo-Si and allo-Ge polymorphs. *J. Phys. Chem. B* **106,** 3402–3409 (2002).
29. Cundy, C. S. & Cox, P. A. The hydrothermal synthesis of zeolites: History and development from the earliest days to present time. *Chem. Rev.* **103,** 663–701 (2003).
30. San-Miguel, A. *et al.* High pressure behavior of silicon clathrates: A new class of low compressibility materials. *Phys. Rev. Lett.* **83,** 5290–5293 (1999).
31. Tritt, T. M. *Semiconductors and Semimetals* Vol. 69 (Academic, 2001).
32. Tauc, J., Grigorovici, R. & Vancu, A. Optical properties and electronic structure of amorphous germanium. *Phys. Status Solidi* **15,** 627–637 (1966).
33. Salpeter, E. E. & Bethe, H. A. A relativistic equation for bound-state problems. *Phys. Rev.* **84,** 1232–1242 (1951).
34. Albrecht, S., Reining, L., Sol, R. D. & Onida, G. *Ab initio* calculation of excitonic effects in the optical spectra of semiconductors. *Phys. Rev. Lett.* **80,** 4510–4513 (1998).
35. Reference solar spectral irradiance: Air mass 1.5; http://rredc.nrel.gov/solar/spectra/am1.5
36. Alonso, M. I., Wakita, K., Pascual, J., Garriga, M. & Yamamoto, N. Optical functions and electronic structure of $CuInSe_2$, $CuGaSe_2$, $CuInS_2$, and $CuGaS_2$. *Phys. Rev. B* **63,** 075203 (2001).
37. Meng, Y. *et al.* High optical quality multicarat crystal diamond produced by chemical vapor deposition. *Phys. Status Solidi A* **209,** 101–104 (2012).
38. Zwijnenburg, M. A., Illas, F. & Bromley, S. T. Apparent scarcity of low-density polymorphs of inorganic solids. *Phys. Rev. Lett.* **104,** 175503 (2010).
39. Nguyen, M. C., Zhao, X., Wang, C-Z. & Ho, K-M. sp^3-hybridized framework structure of group-14 elements discovered by genetic algorithm. *Phys. Rev. B* **89,** 184112 (2014).

Acknowledgements

The experimental work was supported by DARPA under contract numbers W31P4Q-13-1-0005 and W911NF-11-1-0300. The theoretical work was supported by Energy Frontier Research in Extreme Environments (EFree) Center, an Energy Frontier Research Center funded by the US Department of Energy, Office of Science under award number DE-SC0001057. We thank T. Muramatsu and V. Struzhkin for assistance with electrical measurements, J. Holaday and Y. Kono for helping with experimental synthesis, J. Armstrong for support with SEM measurements, and J. Smith, B. Baptiste and H. Gou for help with XRD. Facilities and infrastructure support were provided by the following. Portions of this work were performed at HPCAT (Sector 16), Advanced Photon Source (APS), Argonne National Laboratory. HPCAT operations are supported by DOE-NNSA under Award No. DE-NA0001974 and DOE-BES under Award No. DE-FG02-99ER45775, with partial instrumentation funding by NSF. The Advanced Photon Source is a US Department of Energy (DOE) Office of Science User Facility operated for the DOE Office of Science by Argonne National Laboratory under Contract No. DE-AC02-06CH11357. X-ray diffraction facilities at the Geophysical Laboratory were supported, in part, by the WDC Research Fund. Na_4Si_{24} precursor synthesis experiments with *in situ* XRD were performed at the ID06 beamline at the European Synchrotron Radiation Facility (ESRF), Grenoble, France. We are grateful to W. Crichton, J. Guignard and Y. Le Godec for providing assistance in using this beamline.

Author contributions

D.Y.K. performed all theoretical calculations. S.S., O.O.K. and T.A.S. performed all experimental synthesis and characterization. All authors discussed the results and contributed to the manuscript.

Additional information

Supplementary information is available in the online version of the paper. Reprints and permissions information is available online at www.nature.com/reprints. Correspondence and requests for materials should be addressed to T.A.S.

Competing financial interests

The authors declare that they have filed a provisional patent application.